BIOCHEMISTRY
including biophysical chemistry & molecular biology
Article

Biochemistry **2010,** *49,* 9533–9541 9533
DOI: 10.1021/bi101407m

The Association−Dissociation Behavior of the ApoE Proteins: Kinetic and Equilibrium Studies[†]

Kanchan Garai and Carl Frieden*

Department of Biochemistry and Molecular Biophysics, Washington University School of Medicine, St. Louis, Missouri 63110, United States

Received August 31, 2010; Revised Manuscript Received October 4, 2010

ABSTRACT: The apolipoprotein E family consists of three major protein isoforms: apolipoprotein E4 (ApoE4), ApoE3, and ApoE2. The isoforms, which contain 299 residues, differ only by single-amino acid changes, but of the three, only ApoE4 is a risk factor for Alzheimer's disease. At micromolar concentrations, lipid-free ApoE exists predominantly as tetramers. In more dilute solutions, lower-molecular mass species predominate. Using fluorescence correlation spectroscopy (FCS), intermolecular fluorescence resonance energy transfer (FRET), and sedimentation methods, we found that the association−dissociation reaction of ApoE can be modeled with a monomer−dimer−tetramer process. Equilibrium constants have been determined from the sedimentation data, while the individual rate constants for association and dissociation were determined by measurement of the kinetics of dissociation of ApoE and are in agreement with the equilibrium constants. Dissociation kinetics as measured by intermolecular FRET show two phases reflecting the dissociation of tetramer to dimer and of dimer to monomer, with dissociation from tetramer to dimer being more rapid than the dissociation from dimer to monomer. The rate constants differ for the different ApoE isoforms, showing that the association−dissociation process is isoform specific. Strikingly, the association rate constants are almost 2 orders of magnitude slower than expected for a diffusion-controlled process. Dissociation kinetics were also monitored by tryptophan fluorescence in the presence of acrylamide and the data found to be consistent with the monomer−dimer−tetramer model. The approach combining multiple methods establishes the reaction scheme of ApoE self-association.

The apolipoprotein E (ApoE)[1] family consists of three major isoforms (ApoE4, ApoE3, and ApoE2), with the only differences being arginine to cysteine mutations at positions 112 and 158. ApoE4 has arginines at both these positions; ApoE2 has cysteines at both these positions, and ApoE3 has a cysteine at position 112 and an arginine at position 158. ApoE4, however, is known to be the major risk for Alzheimer's disease, while ApoE2 appears to be protective (*1*−*4*). The complete structure of wild-type ApoE is unknown, but the ApoE monomer consists of two domains, an N-terminal domain (residues 1−191) and a C-terminal domain (residues 221−299) (*5*, *6*) with the arginine to cysteine changes occurring in the N-terminal domain. The two domains are linked by a 40-amino acid protease sensitive hinge region. Lipid-free protein at micromolar or higher concentrations exists primarily as a tetramer, although small amounts of higher-molecular mass forms may be present (*6*−*11*), while at lower concentrations, the protein dissociates to a monomeric form. The molecular mass distribution of these forms is not clear, and no structure of any oligomeric form is known. Unlike the N-terminal domain, the isolated C-terminal domain of ApoE oligomerizes, and hence, this domain is thought to mediate ApoE oligomerization (*7*, *11*, *12*). Zhang et al. introduced four or five mutations into the C-terminal domain of ApoE3 that prevented aggregation of both the C-terminal domain (*13*) and full-length ApoE3 (*14*). The C-terminal region, however, is thought to contain the major lipid binding site (*7*), and the mutations that prevent self-association also result in more rapid lipoprotein particle formation from DMPC vesicles (*14*). These observations suggest that there may well be a correlation between lipid binding and the association−dissociation process. The role of the N-terminal region in self-association and lipid binding is unknown.

There have been efforts to characterize the self-association behavior of ApoE molecules, primarily using sedimentation methods (*10*, *11*, *15*, *16*). With the recent advances in the data analysis of the sedimentation experiments, it has been possible to determine the equilibrium constants of the self-association process of ApoE assuming a monomer−dimer−tetramer−octamer model (*10*, *16*). However, the determination of the individual association and dissociation rate constants is not possible from sedimentation data and requires kinetic experiments. While there are many examples of measurements of association and dissociation rate constants for monomer−dimer or monomer−oligomer systems (*17*−*24*), there appear to be no direct measurements of these rate constants for more complicated systems involving three species. Rate constants, however, are important and have been informative in many cases involving protein−protein interactions (*18*, *23*−*25*).

Here we use fluorescence correlation spectroscopy (FCS) and sedimentation methods to characterize the overall self-association

[†]This research was supported in part by National Institutes of Health Grant DK13332.

*To whom correspondence should be addressed. E-mail: frieden@biochem.wustl.edu. Phone: (314) 362-3344. Fax: (314) 362-7183.

[1]Abbreviations: ApoE, apolipoprotein E; WT, wild type; serine mutant of ApoE3, apolipoprotein E3 (C112S); serine mutant of ApoE2, apolipoprotein E2 (C112S/C158S); monomeric form of ApoE4, apolipoprotein E4 (F257A/W264R/V269A/L279Q/V287E); GdnCl, guanidine hydrochloride; FCS, fluorescence correlation spectroscopy; FRET, fluorescence resonance energy transfer; βMe, β-mercaptoethanol.

Published on Web 10/05/2010

states of ApoE. The kinetics of dissociation are measured by changes in intermolecular FRET and show two phases reflecting tetramer to dimer and dimer to monomer processes. The simplest model that fits the data is that of a monomer to dimer to tetramer association. Individual rate constants for the association and dissociation reactions are determined from these data. The association rate constants are slower than what would be expected from simple diffusion-controlled reactions. This appears to be the first explicit determination of rate constants for a complex reaction system involving monomer, dimer, and tetramer.

MATERIALS AND METHODS

Expression and Purification of ApoE. Apolipoprotein E was prepared and purified as described elsewhere (*26*). Site-directed mutations were introduced by using the site-directed mutagenesis kit from Qiagen. The sequences of mutant proteins were verified by DNA sequencing.

Fluorescence Labeling of ApoE's. The cysteine residue(s) of WT ApoE2 and WT ApoE3 were replaced with serine. The alanine at position 102 in each isoform was mutated to cysteine for fluorescent labeling. Thus, all the ApoE isoforms contained a single cysteine residue at position 102. ApoE forms containing this cysteine were labeled with either Alexa488 maleimide or Alexa546 maleimide (Invitrogen). The protein at 2 mg/mL was dissolved in 50 mM HEPES buffer (pH 7.4), 6 M urea, and 200 μM tris (2-carboxyethyl)phoshine (TCEP). The solution was degassed under vacuum for 20 min. The maleimide dye (200 μM) was added and the solution kept in the dark at room temperature under vacuum for 2 h. The reaction mixture was then kept at 4 °C over night. Excess dye was removed when the sample was passed over a Superdex200 column in 4 M GdnCl (guanidine HCl), 20 mM HEPES buffer (pH 7.4), and 0.1% β-mercaptoethanol (βMe). The labeled ApoE was then refolded by dialysis against 20 mM HEPES buffer (pH 7.4) and 150 mM NaCl at 4 °C overnight. The absorbance of this sample at 280 and 490 nm (for Alexa488) or 555 nm (for Alexa546) was used to determine the extent of labeling. For all the samples, the extent of labeling was greater than 90%.

Fluorescence Correlation Spectroscopy. FCS measurements were performed on a Confocor 2 microscope equipped with FCS capability (Zeiss Inc., Jena, Germany). The FCS autocorrelation data were fit to eq 1a to obtain the diffusion time, τ_D (*27*−*29*).

$$G(t) = \frac{1}{N}\left(1+\frac{t}{\tau_D}\right)^{-1}\left(1+\frac{t}{\omega^2\tau_D}\right)^{-0.5}\frac{1-A+A\exp(-t/\tau_A)}{1-A} \tag{1a}$$

where ω is the experimentally measured axial ratio of the FCS observation volume, N is the number of molecules and τ_D the diffusion time in the FCS observation volume, A is the amplitude, and τ_A is the time of any relaxation process taking place. The diffusion coefficient of ApoE (D_{ApoE}) was calculated from the experimentally obtained diffusion times, τ_D, using eq 1b.

$$D_{ApoE} = \frac{D_{Alexa488}\tau_{Alexa488}}{\tau_{ApoE}} \tag{1b}$$

The diffusion coefficient of Alexa488 dye (*30*) in water ($D_{Alexa488}$) equals 4.3×10^{-6} cm^2/s.

The kinetic assessment of oligomer dissociation was performed by FCS using 100-fold dilution of a 20 μM Alexa488-labeled (at position 102) ApoE4 solution. Data obtained at each time point were averaged for 3 min. The diffusion coefficient of monomeric ApoE was determined by FCS using the Alexa488-labeled monomeric form of ApoE4 at 200 nM (*14*). Prior to FCS measurement, the protein was passed through a Superdex200 column in 20 mM HEPES buffer (pH 7.4) and 150 mM NaCl and the monomeric fraction used. To measure the concentration dependence of the diffusion coefficient, 100 nM Alexa488-labeled ApoE4 was mixed with varying concentrations of wild-type ApoE4 ranging from 100 nM to 10 μM. The samples were incubated overnight in glass coverslip bottom eight-well chambered cells (Nunc) at room temperature. FCS measurements were performed the next day to determine the concentration dependence of the diffusion coefficient. The molecular masses of ApoE (M_{ApoE}) were calculated using eq 1c

$$M_{ApoE} = \left(\frac{D_{ApoE}}{D_{monomericApoE}}\right)^{-3} \times 34.2\ \text{kDa} \tag{1c}$$

Sedimentation Equilibrium Experiments and Data Analysis. A Beckman Optima model XL-A analytical ultracentrifuge was used for all sedimentation experiments. Samples (100 μL) and reference (120 μL) solutions were loaded into a conventional double-sector filled Epon centerpiece (path length of 1.2 cm). Data were collected at 280 nm with five averages, at time intervals of 240 min and radial intervals of 0.001 cm, until sedimentation equilibrium was attained. Experiments were conducted at 20 °C with a rotor velocity of 10000 rpm. Molar extinction coefficients at 280 nm (44500 M^{-1} cm^{-1}) and partial specific volumes (v) of ApoE3 and ApoE4 (0.732 mL/g) were assumed. The sample concentrations used were 4 and 8 μM in 100 mM NH_4HCO_3. The data were analyzed with a continuous mass distribution using SEDFIT (*31*, *32*).

Sedimentation Velocity Experiments and Analysis. Sedimentation velocity experiments were conducted at 20 °C at a rotor speed of 40000 rpm. Data were collected in continuous mode, at a single wavelength, using a time interval of 300 s and a step size of 0.002 cm without averaging. The experiments were performed with 2, 4, and 8 μM ApoE in 100 mM NH_4HCO_3 buffer. Multiple scans at different time points were fitted to a monomer−dimer−tetramer rapid self-association model using SEDFIT (*31*, *32*). In SEDFIT, the equilibrium constants K_{12} and K_{14} are obtained in the absorbance unit and were converted to concentration by eq 2a.

$$K_{12}^{abs} = \frac{2K_{12}^{molar}}{\varepsilon_{monomer}} \quad \text{and} \quad K_{14}^{abs} = \frac{4K_{14}^{molar}}{\varepsilon_{monomer}{}^3} \tag{2a}$$

where $\varepsilon_{monomer}$ is the extinction coefficient of the protein at 280 nm (44500 M^{-1} cm^{-1}). The equilibrium constant from the dimer to the tetramer, $K_{24}{}^{molar}$ is calculated using eq 2b.

$$K_{24}^{molar} = \frac{K_{14}^{molar}}{(K_{12}^{molar})^2} \tag{2b}$$

Passivation of Cuvette Surface. To avoid adsorption of ApoE to the surface of a cuvette, the inner surface was passivated using the method of Selvin and Ha (*33*). Briefly, the quartz cuvette was thoroughly cleaned and then functionalized with (3-aminopropyl)triethoxysilane (Sigma). The surface passivation reaction was conducted with methoxy-poly(ethylene glycol)-succinimidyl valerate (mPEG-SVA, Laysan Bio Inc.) in bicarbonate buffer (pH 8.3).

FRET Experiments. ApoEs labeled with either Alexa488 or Alexa546 were mixed at a ratio of 1:3 in 4 M GdnCl. This sample

Scheme 1: Self-Association Monomer−Dimer−Tetramer Model of ApoE[a]

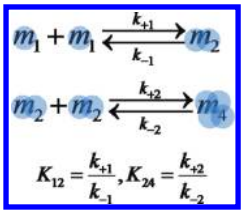

[a] m_1, m_2, and m_4 represent monomer, dimer, and tetramer, respectively. K_{12} and K_{24} are equilibrium constants for the monomer to dimer and dimer to tetramer association processes, respectively.

was then dialyzed at 4 °C in 20 mM HEPES buffer (pH 7.4) and 150 mM NaCl, flash-frozen in liquid nitrogen in small aliquots (100 μL), and then stored at −80 °C prior to use. Before the FRET experiment, a 400 μL stock solution (concentration of ≈15 μM) was incubated overnight at room temperature in an eight-well chamber glass coverslip bottom cell. The FRET kinetic experiments were performed using an Alphascan fluorometer (Photon Technology International, Inc.) equipped with a programmable shutter with the excitation and emission monochromators set at 490 and 520 nm, respectively. Different amounts of the ApoE stock solution (from 1.5 to 100 μL) were added to 3 mL of buffer and mixed within 2−3 s. The fluorescence was then monitored for 1 h. To minimize photobleaching, the shutter in the excitation light path was closed between measurements. All experiments were performed at 24 °C.

Monomer−Dimer−Tetramer Association Model and Data Fitting. The kinetic data from the FRET experiments were globally fit to a monomer−dimer−tetramer association model (shown in Scheme 1) using Kinetic Explorer Software version 2.2.563 (Kintek Corp.) (*34*). The experimental observable, i.e., the donor dye fluorescence, $F(t)$, is expressed as $F(t) = c(m_1 + e_2m_2 + e_4m_4)$, where c is a normalization constant and e_2 and e_4 are the average relative (compared to the monomers) brightness values of the dimers and tetramers, respectively. Experiments were simulated in two steps: first equilibration of the stock solution (monomeric concentration of ≈15 μM) and then dilution of this solution (for most experiments, dilutions are 1000-, 500-, 250-, 125-, and 62.5-fold). The initial distribution of the monomers, dimers, and tetramers in the stock solution was calculated using the same set of rate constants that describes the kinetics of monomer and dimer formation due to dilution. The kinetic data from all the dilutions were fit globally to obtain the four rate constants and two brightness values. Kintek Explorer FitSpace was used to determine how well constrained the rate constants were (*35*).

Tryptophan Fluorescence Quenching Kinetics Experiments. For these experiments, WT ApoE4, ApoE3, or ApoE2 was used. A 400 μL stock solution (concentration of ≈25 μM) was incubated overnight at room temperature in an eight-well chamber glass coverslip bottom cell. The excitation and emission monochromators in the fluorometer were set to 290 and 340 nm, respectively. Different amounts of ApoE (from 3 to 12 μL) were added to 3 mL of HEPES buffer and mixed within 2−3 s in buffer containing 100 mM acrylamide. The fluorescence data were then recorded for 1 h.

RESULTS

Dissociation of ApoE Using FCS. At micromolar protein concentrations, ApoE exists primarily as a tetramer (*9*, *10*). Figure 1 shows how the diffusion coefficient changes with time after a 20 μM

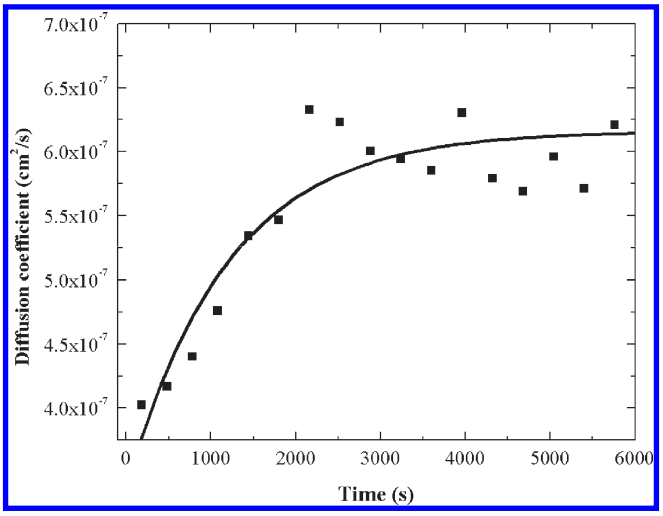

FIGURE 1: Dissociation of ApoE4 measured by FCS. Time dependence of dissociation of ApoE4 after dilution followed by FCS. Alexa488-labeled ApoE4 (20 μM) was diluted 100-fold into 20 mM HEPES buffer (pH 7.4), 150 mM NaCl, and 0.1% βMe. The solid line is a single-exponential fit of the data. The diffusion coefficients of ApoE were calculated from diffusion times using eq 1b.

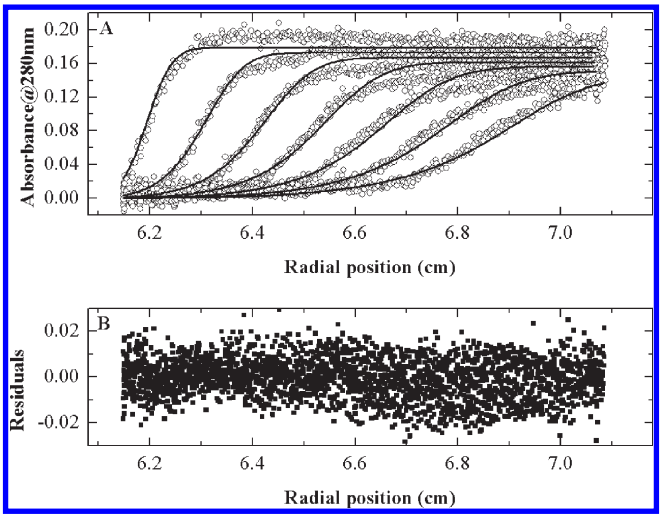

FIGURE 2: Sedimentation velocity experiments using WT ApoE4. (A) Data from sedimentation velocity experiments using 4 μM WT ApoE4. The solid lines are fits to a monomer−dimer−tetramer model as discussed in the text. (B) Residuals of the fit.

Alexa488-labeled ApoE4 solution is diluted 100-fold to a final concentration of 200 nM. The data can be fit by a single exponential with an observed half-time of ≈1200 s, and the increase in the diffusion coefficient after dilution implies a decrease in the average molecular mass and is a direct indication of the dissociation of the ApoE oligomers. The data show that the dissociation is slow but do not allow a determination of any reaction model.

Sedimentation Velocity. Sedimentation velocity experiments were performed at 2, 4, and 8 μM WT ApoE4. As we will discuss in the following section, our kinetic data cannot be fit by simple monomer−dimer or dimer−tetramer systems. Therefore, to interpret the sedimentation velocity data, we assumed the next simplest model, a monomer−dimer−tetramer association model that is shown in Scheme 1. Figure 2A shows the data (○) and fits (—) using SEDFIT (*31*, *32*) using a monomer−dimer−tetramer model. Figure 2B shows the residuals of the fit. The concentration of ApoE4 for this experiment was 4 μM. The fits converged to sedimentation coefficients of 2.82, 3.93, and 7.18 S for the

Table 1: Summary of Rate and Equilibrium Constants

sample	experiment	k_{+1} (M^{-1} s^{-1})	k_{-1} (s^{-1})	k_{+2} (M^{-1} s^{-1})	k_{-2} (s^{-1})	K_{12}^{-1} (M)	K_{24}^{-1} (M)
WT ApoE4	sedimentation velocity					140×10^{-9}[a]	89×10^{-9}[a]
ApoE4 (A102C)	kinetics	8.5×10^{3}	6.7×10^{-4}	2.0×10^{5}	4.0×10^{-3}	79×10^{-9}[b]	22×10^{-9}[b]
ApoE3 (C112S/A102C)	kinetics	4.7×10^{3}	5.6×10^{-4}	0.8×10^{5}	5.0×10^{-3}	119×10^{-9}[b]	62×10^{-9}[b]
ApoE2 (C112S/C158S/A102C)	kinetics	6.0×10^{3}	6.6×10^{-4}	0.8×10^{5}	3.6×10^{-3}	110×10^{-9}[b]	45×10^{-9}[b]

[a]These are converted to molar units using eq 1 from the equilibrium constants obtained in absorbance units. [b]These are calculated from k_{+1}, k_{-1}, k_{+2}, and k_{-2} using the formulas given in Scheme 1.

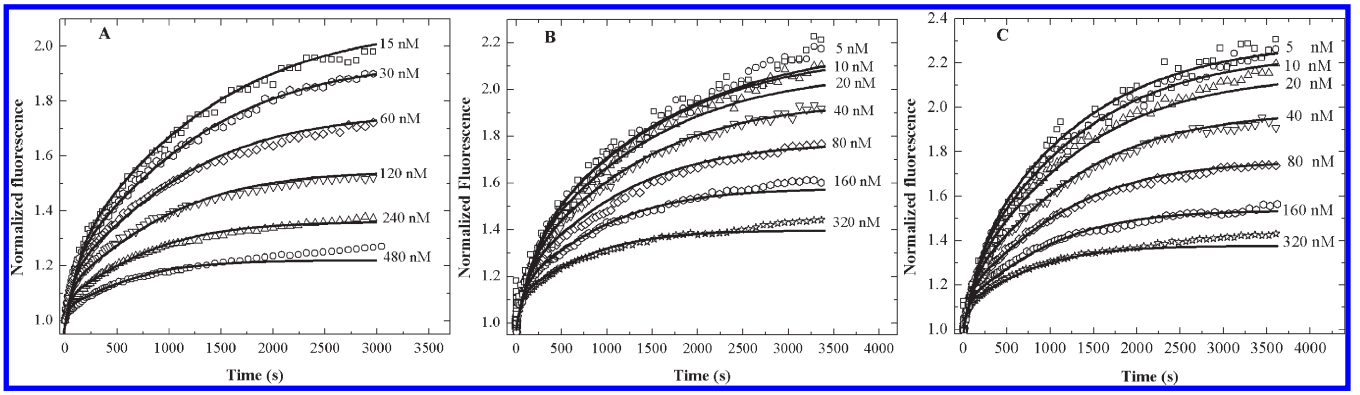

FIGURE 3: Kinetics of dissociation of Alexa488- and Alexa546-labeled ApoE isoforms using intermolecular FRET. Fluorescently labeled ApoE (15 μM) was diluted into 20 mM HEPES buffer (pH 7.4), 150 mM NaCl, and 0.1% βMe to various final concentrations as indicated in the figures. The symbols represent data from ApoE4 (A), the serine mutant of ApoE3 (C112S) (B), and ApoE2 (C112S/C158S) (C), and the solid lines are fits to a monomer−dimer−tetramer model using Kintek Explorer (*35*). The rate constants obtained are listed in Table 1. The ratio of Alexa488-labeled ApoE to Alexa546-labeled ApoE is 1:3. The fluorescence was monitored at 520 nm with excitation at 490 nm.

monomer, dimer, and tetramer, respectively. The equilibrium constants K_{12} and K_{24} are summarized in Table 1.

Kinetics of Dissociation of ApoE Using FRET. Using changes in intermolecular FRET, we determined the kinetics of the dissociation process. When Alexa488- and Alexa546-labeled ApoE's are mixed, the fluorescence of Alexa488 is quenched in a concentration-dependent manner (Figure S1 of the Supporting Information), an indication of intermolecular FRET due to self-association of ApoE molecules. Following dilution, the fluorescence of the donor increased with time due to re-equilibration of the oligomeric forms. Experiments as a function of the final concentration of the protein allow a unique fit of both the dissociation and association rate constants. Figure 3A shows the data (symbols) for the time course of the donor fluorescence from ApoE4 after dilution from higher to lower concentrations. The starting concentration of ApoE4 was 15 μM, and the final concentrations were 15, 30, 60, 120, 240, and 480 nM as shown in Figure 3A. As discussed in Materials and Methods, the ratio of ApoE's labeled with either Alexa488 or Alexa546 was 1:3. For visual comparison, the data in Figure 3A were normalized to the fluorescence at time zero. Attempts to fit the kinetic data with a monomer−dimer or dimer−tetramer model were unsuccessful. Therefore, the next simplest model of a monomer to dimer to tetramer association was used to fit the data. The solid black lines in Figure 3A are global fits of all the data using a monomer−dimer−tetramer model. The rate constants obtained are listed in Table 1. The equilibrium constants calculated from the association and dissociation rate constants are consistent with those obtained from the sedimentation velocity experiments. Panels B and C of Figure 3 show similar kinetic experiments performed with ApoE3 (C112S/A102C) and ApoE2 (C112S/C158S/A102C). Here, to have the fluorescent probes at the same position in all the isoforms, we substituted the cysteine residue(s) of these proteins with serine(s) for these experiments and mutated alanine 102 to cysteine. The concentrations used for these samples are similar to those of ApoE4 and are shown in the figures. All the data have been fit to the same model. Fits to the data appear quite reasonable over the concentration range from 5 to 240 nM for all the ApoE isoforms. There is a slight deviation from the fits at 480 nM, which may be due to the presence of small amounts of higher-molecular mass forms at this concentration. As discussed later, a striking feature is that the equilibration process is very slow, taking more than 1 h after dilution to be completed.

Figure 4 shows the correlation plots of the rate constants obtained for the ApoE3 serine mutant using the FitSpace program of Johnson et al. (*35*). As discussed by Johnson (*35*), such plots provide a good way to examine the errors involved in the determination of these parameters and to examine the quality of fitting (i.e., same χ^2) by interadjustment of the parameters. In these two-dimensional plots, the red regions correspond to the best fit (i.e., minimum χ^2 of data fitting) values of the rate constants and the yellow boundaries indicate standard errors (corresponding to $1.3\chi^2_{min}$) in the parameters. It can be seen from the figure that the values of the dissociation rate constants, k_{-1} and k_{-2}, are tightly constrained within $\pm 10^{-4}$ and $\pm 10^{-3}$ s^{-1}, respectively. The values of the association rate constants, k_{+1} and k_{+2}, vary from $(4.7 \pm 1.7) \times 10^3$ to $(0.80 \pm 0.26) \times 10^5$ M^{-1} s^{-1}. Although k_{+1} and k_{+2} contain larger errors, it is clear from the FitSpace plots that all four rate constants are constrained within bounds. In general, if more rate constants than necessary are used to describe the data, then the FitSpace plots would show that at least some of the rate constants would be out of bounds. The fact that this does not happen for our model indicates that this model is optimal for describing the kinetic data. It may be noted that the level of confidence in the determination of the rate constants is improved via inclusion of more experimental data; hence, at least five

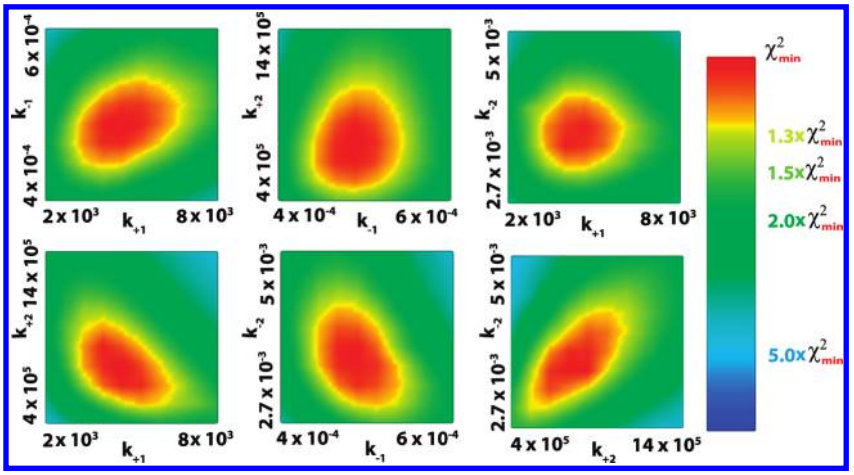

FIGURE 4: FitSpace plot of the rate constants. FitSpace plot of the fit of the data shown in Figure 3B of the serine mutant of ApoE3 (C112S). The FitSpace plot is computed around the best fit parameter values using Kintek Explorer (*35*). The axes represent the values of the particular rate constants, k_+ or k_-, expressed in M^{-1} s^{-1} or s^{-1}, respectively. In these two-dimensional plots, the values of χ^2 are presented in colors. The column at the right shows the color scale of χ^2 with respect to $\chi_{minimum}{}^2$. The yellow contours represent the confidence intervals of the rate constants. The presence of finite contours in all the plots indicates that the monomer−dimer−tetramer model adequately describes the kinetic data and that the values of the rate constants are unique.

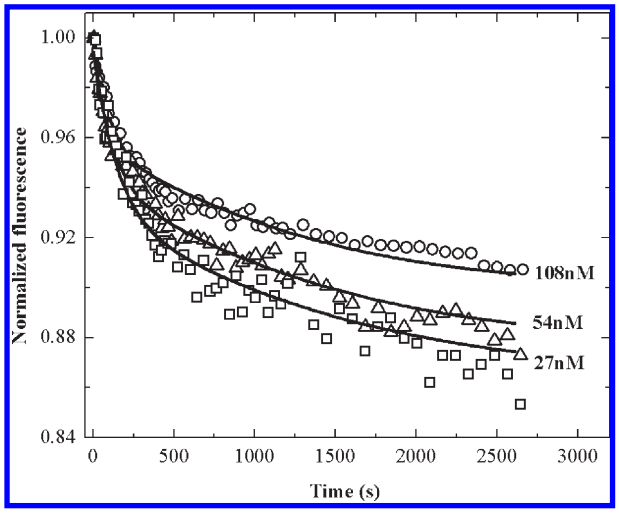

FIGURE 5: Kinetics of dissociation of WT ApoE3 using acrylamide quenching of tryptophan fluorescence. WT ApoE3 (27 μM) was diluted into 20 mM HEPES buffer (pH 7.4), 150 mM NaCl, and 0.1% βMe in the presence of 100 mM acrylamide to final concentrations of 27, 54, and 108 nM. The squares, triangles, and circles represent experimental data at different concentrations, and the solid lines are simulated using the rate constants listed in Table 1 obtained for the serine mutant of ApoE3. The fluorescence is monitored at 340 nm with excitation at 290 nm.

to seven dilution experiments were performed for each ApoE isoform.

Kinetics of Dissociation of ApoE Using Acrylamide Quenching. The ApoE monomer contains seven tryptophan residues, four in the N-terminal domain and three in the C-terminal domain. Our previous ^{19}F NMR experiments suggested that the tryptophan residues in the C-terminal domain and one tryptophan in the N-terminal domain are solvent-exposed in the monomeric protein (*26*). In the presence of acrylamide, the tryptophan fluorescence is quenched in a way such that the extent of quenching is dependent on ApoE concentration, suggesting that some of these residues may be at least partially buried in the dimer and the tetramer (Figure S2 of the Supporting Information). This observation allowed us to monitor the association and dissociation of ApoE by tryptophan quenching using WT ApoE rather than fluorescently labeled protein. Figure 5 shows the time course of the tryptophan fluorescence after dilution of WT ApoE3 into 20 mM HEPES buffer (pH 7.4) and 150 mM NaCl containing 100 mM acrylamide. The concentration of the acrylamide used was chosen from a Stern−Volmer plot to ensure that the nature of the quenching is dynamic and not static (data not shown). The initial concentration of ApoE3 was 27 μM, and final concentrations were 27, 54, and 108 nM as shown in the figure. The lines are simulated curves using the monomer−dimer−tetramer model and the same rate constants obtained from the fitting of the FRET data of the ApoE3 serine mutant (Table 1). Similar experiments have been performed using WT ApoE2 and WT ApoE4 (data not shown), and the data agree well with the rate constants listed in Table 1 for the ApoE2 serine mutant and ApoE4, respectively. We infer from these results that the cysteine to serine mutations in both ApoE3 and ApoE2 do not significantly affect their association and dissociation rate constants. Fluorescence labeling of ApoE at position 102 also appears not to significantly interfere with the properties of ApoE.

Measurement of Diffusion Coefficients of ApoE as a Function of Concentration. Figure 6 shows a plot of the molecular mass of ApoE4 molecules with concentrations ranging from 200 nM to 10 μM. Molecular masses are calculated using eq 1c, from the measured diffusion coefficients using a molecular mass of the monomer of 34200 Da and a diffusion coefficient of 7.6×10^{-7} cm^2/s, the latter value being determined by FCS using a monomeric form of ApoE4 (*14*). The solid black line is obtained using the association and dissociation rate constants obtained for ApoE4 from the kinetic experiments as summarized in Table 1. It is apparent from this figure that there is good agreement between the data obtained from the two different methods.

Sedimentation Equilibrium. Figure 7A shows the sedimentation equilibrium data (symbols) obtained at 4 and 8 μM WT ApoE4. The data were fit to a continuous mass distribution using SEDFIT (*31*, *32*). Figure 7B shows the residuals of the fits. The mass distribution obtained is wide, ranging from 90 to 150 kDa (Figure 7C). The mean molecular masses for 4 and 8 μM ApoE4 are 115 and 128 kDa, respectively (Figure 7C). These mean molecular mass values, plotted as empty circles in Figure 6, are consistent

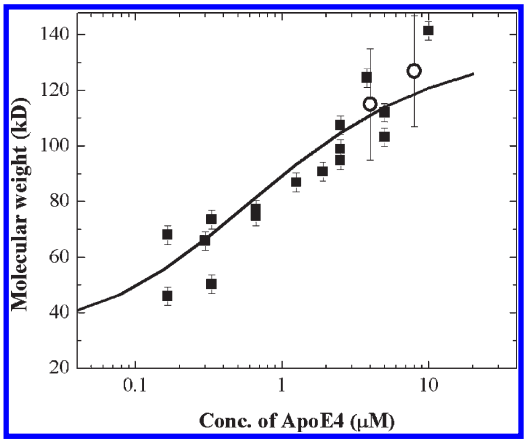

FIGURE 6: Mean molecular mass of ApoE4 as a function of concentration. The black squares represent mean molecular masses obtained from FCS measurements of WT ApoE4. Alexa488-labeled ApoE4 (100 nM) was present in all the samples. The molecular masses were calculated from the diffusion coefficients using eq 1c. The diffusion coefficient of monomeric ApoE4 used in the calculation was 7.6×10^{-7} cm^2/s as determined by FCS. The empty circles represent molecular masses obtained from sedimentation equilibrium experiments (see Figure 7). The solid curve was calculated using Kintek Explorer (*34*) from the rate constants listed in Table 1 for ApoE4 obtained from kinetic experiments.

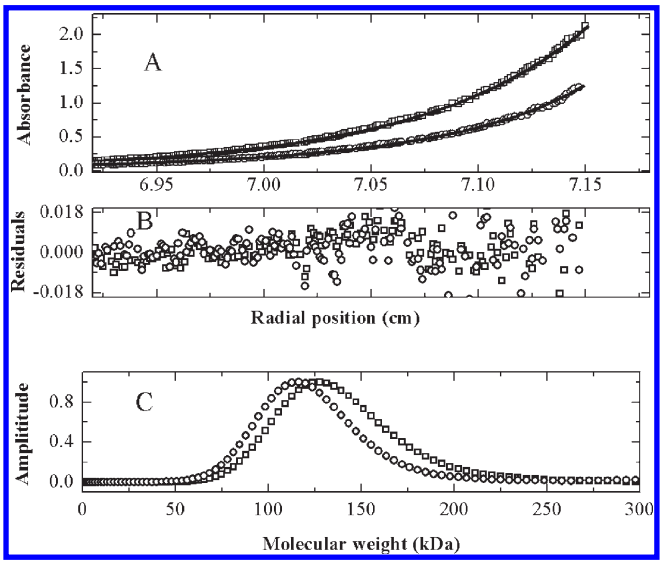

FIGURE 7: Sedimentation equilibrium experiments with WT ApoE4. The concentrations of WT ApoE4 used were 4 (○) and 8 μM (□). (A) Sedimentation data and fit with continuous mass distribution using SEDFIT (*31*, *32*). (B) Residuals of the fit. (C) Mass distribution obtained from the fit. The mean molecular masses for 4 and 8 μM ApoE4 are 114 and 129 kDa, respectively.

with the values obtained from the other two methods and also are consistent with the reported values (*9*, *10*).

DISCUSSION

Rationale for the Monomer−Dimer−Tetramer Model. As mentioned earlier, we were unable to fit the kinetic data with a simple monomer−dimer or dimer−tetramer association scheme. The monomer−dimer−tetramer model was successful in fitting both the sedimentation data and the kinetic data. The validity and the power of this model are illustrated by the fact that the same set of rate constants can fit the data over a large concentration range [viz., from 5 to 480 nM (see Figure 3A−C)]. Furthermore, several independent methods are consistent with a monomer−dimer−tetramer model and with the rate constants derived from the dissociation kinetics. The kinetic data reveal two distinct phases with the faster rate corresponding to dissociation from the tetramer to dimer and the slower rate to the subsequent dissociation of dimers to monomers. Our results do not rule out the possibility of the presence of the forms larger than tetramers that have been observed by several authors (*9*, *10*, *36*), but the population of these larger forms must be small under the experimental conditions used here.

It is interesting to note that while there are kinetic data in the literature for determining rate constants for the monomer−dimer or monomer−tetramer system (*18*, *23*−*25*, *37*−*41*), there do not appear to be kinetic data for a monomer−dimer−tetramer system. The data presented here solve that problem by employing complementary techniques.

Differences between the Isoforms. Table 1 shows that the association and dissociation rate constants for ApoE4, ApoE3, and ApoE2 are different. The differences between the isoforms are visualized more clearly via comparison of the absolute populations of the monomer, dimer, and tetramer at the same total ApoE concentrations. Figure 8 shows the plots of monomer (Figure 8A), dimer (Figure 8B), and tetramer (Figure 8C) populations for ApoE4, ApoE3, and ApoE2. These populations are estimated using Kintek Explorer using the rate constants obtained from the FRET kinetics measurements as summarized in Table 1. As expected from the rate constants, there are differences between the ApoE isoforms. Although these differences are not large, the differences are more apparent for the monomers and the dimers than for the tetramers. At any specific concentration, ApoE3 has the largest amount of monomeric and dimeric species followed by ApoE4 and ApoE2. Figure 8D shows the plot of the percentage of monomer, dimer, and tetramer population as a function of ApoE4 concentration, ranging from 10 nM to 20 μM. The plot shows that the monomers predominate at ApoE concentrations of < 100 nM while tetramers predominate at $> 2.5\,\mu$M. The dimer population reaches a maximum at $\approx$100 nM and is never the predominant species. The real differences between the ApoE isoforms may lie in their monomer and dimer populations. This is particularly relevant at $\leq$200 nM. It may be noted that the concentration of ApoE in the cerebrospinal fluid (CSF) is $\approx$150 nM (*42*). Because ApoE in CSF exists as lipoprotein complexes, it is not possible to say if the comparison is relevant.

Consistency of the Rate Constants from Different Measurements. Our data from FCS, sedimentation velocity, and kinetic measurements are all consistent with the monomer−dimer−tetramer association model. However, as mentioned earlier, the values of the parameters obtained from the different measurements may differ because of the fact that mutants of ApoE and labeling with fluorophores have been used. The equilibrium constants K_{12} and K_{24} for ApoE4 listed in Table 1 from sedimentation velocity and kinetic experiments are quite close although not exactly the same. Kinetic data from tryptophan quenching experiments agree well with rate constants obtained from the FRET measurements. In addition, it is apparent from Figure 6 that the molecular mass as a function of concentration obtained from FCS, sedimentation equilibrium, and kinetic experiments agree quite well. Figure 8D demonstrates that the average molecular mass approaches that of a tetramer for ApoE concentrations of $> 2\,\mu$M. This is in agreement with our data (Figure 6) as well as published sedimentation equilibrium data (*9*, *10*).

Comparison of the Kinetic Experiments with Sedimentation Velocity. Sedimentation velocity has been widely used to

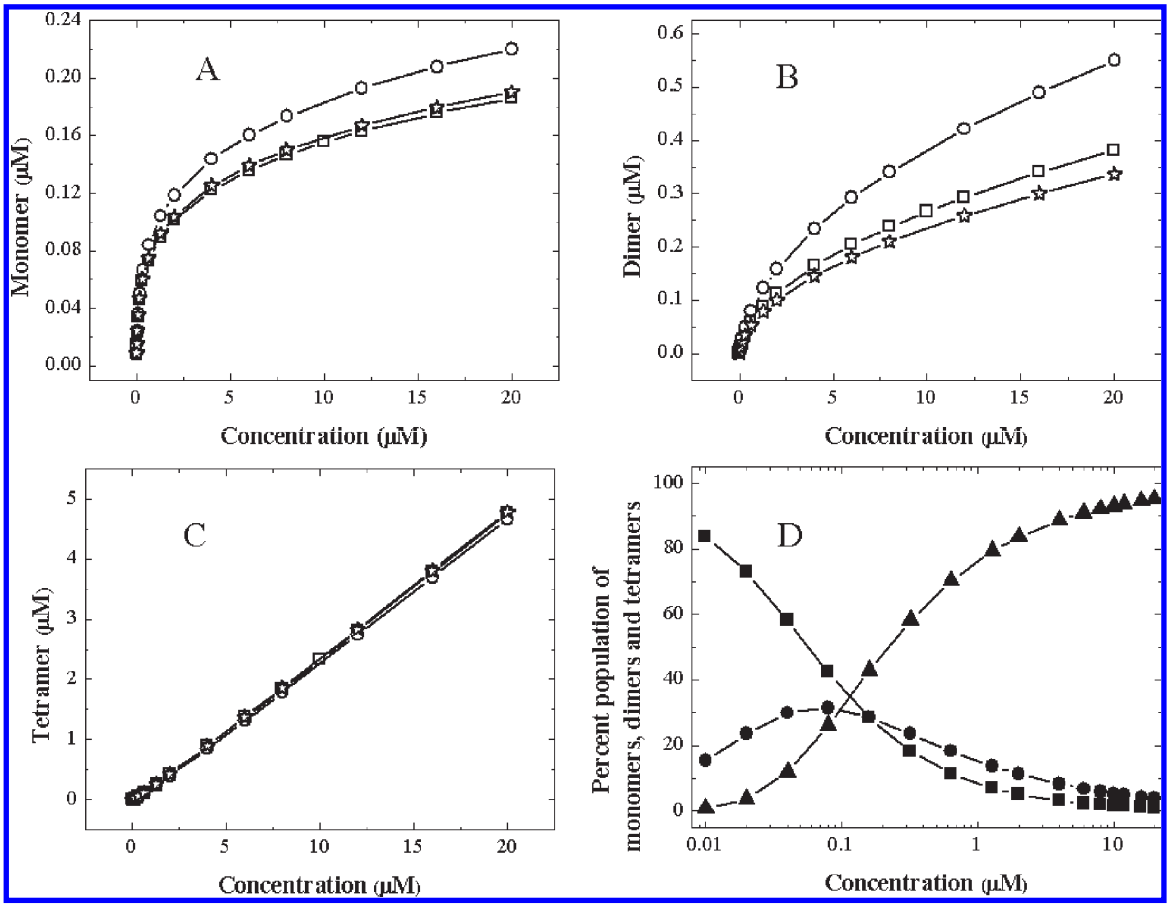

FIGURE 8: Monomer, dimer, and tetramer populations of ApoE isoforms as a function of total concentration. (A−C) Simulations of monomer, dimer, and tetramer populations as a function of the total ApoE concentration for ApoE4 (□), ApoE3 (○), and ApoE2 (☆) respectively. (D) Percent populations of monomers (■), dimers (●), and tetramers (▲) for ApoE4. The simulations were performed using Kintek Explorer (*35*) and the rate constants obtained from kinetics experiments for ApoE4 and serine mutants of ApoE3 and ApoE2 as listed in Table 1.

determine equilibrium constants for two species systems (e.g., monomer−dimer or monomer−tetramer) (*21*, *43*, *44*). Recent improvements in data fitting, especially SEDFIT and SEDPHAT (*31*, *32*), allow fitting of more complicated models such as monomer−dimer−tetramer or monomer−tetramer−octamer models (*45*−*48*). Correct applications of these models require experiments to be performed over a wide range of concentrations over which each of the species is significantly populated. To establish the self-association model of ApoE, sedimentation experiments need to be performed within protein concentrations from ≈50 nM to 2 μM. However, sedimentation experiments with ApoE concentrations of < 1 μM (or 0.03 mg/mL) are difficult because of the low absorbance and adsorption of the sample to the cell walls. On the other hand, kinetic experiments using FRET are possible over this range of protein concentrations. In addition, kinetic data yield both association and dissociation rate constants from which equilibrium constants can be calculated.

Association−Dissociation Rate Constants. The data listed in Table 1 show that the association rate constants are considerably smaller than those expected for diffusion control. Extensive studies using experiments and computations indicate that diffusion-controlled protein−protein association rate constants are on the order of $0.5-5 \times 10^6$ M^{-1} s^{-1} (*37*−*41*). The association rate constants we obtain for ApoE dimer formation and tetramer formation (see Table 1) both are, in general, 10−100-fold slower. This indicates a free energy barrier for formation of both the dimers and the tetramers and may reflect a conformational change necessary for ApoE molecules to self-associate and/or only the presence of a rare form of the monomer or dimer that self-associates. We have no way to distinguish between these two possibilities, although our previous data indicate considerable ApoE heterogeneity (*26*).

Molecular Shape of ApoE. From a diffusion coefficient and a known molecular mass, it is possible to determine the frictional coefficient of the protein. For monomeric ApoE, the diffusion coefficient, measured by FCS, is 7.6×10^{-7} cm^2/s, which is 1.35 times smaller than that expected for a spherical protein with a mass of 34.2 kDa, indicating that the ApoE monomer is not globular but rather has an extended shape with a frictional coefficient of 1.35. This value corresponds to an axial ratio of ∼7 (*49*), close to the value reported by Perugini et al. (*45*). If the frictional coefficient of the tetramer is the same as that of the state of Perugini et al., then the tetramer would appear to be stacked dimers, which in turn would suggest more than one monomer−monomer interface.

Self-Association Behavior and Lipid Binding of ApoE. It should be noted that dimeric and monomeric forms retain structure and that dissociation to these forms from the tetramer may very well open new ligand binding sites. For example, both ApoE self-association and lipid binding have been suggested to be mediated through the C-terminal domain, and if these two processes are linked, then the association−dissociation process of the different isoforms may be relevant. In addition, it is known that the lipid binding kinetics are slow, and we show here that the association−dissociation process is slow as well. As mentioned earlier, the mutations that inhibit self-association in ApoE3 also result in more rapid formation of lipoprotein particles from

DMPC vesicles (*14*). The possibility that these processes are linked makes a compelling argument for understanding the association and dissociation processes of the ApoE isoforms. While the ApoE molecular mass form(s) that binds to lipids is unknown, it is known that ApoE4 is the major risk factor for Alzheimer's disease (*1*−*4*). The question is whether the physiological differences between the different ApoE isoforms may be related to their ability to undergo the association−dissociation reaction.

Conclusions. In summary, using both kinetic and sedimentation data, we have determined the association and dissociation rate constants of the ApoE self-association reactions. It is shown that the different isoforms of ApoE differ with respect to their association−dissociation properties. The association rate constants are much slower than diffusion-controlled reactions, indicating the presence of a barrier in the formation of the oligomeric forms. To the best of our knowledge, it is the first attempt to determine the rate constants in a system involving monomer, dimer, and tetramer and ApoE can act as a model system in characterizing such processes.

ACKNOWLEDGMENT

We thank Berevan Baban for excellent technical assistance and Dr. Roberto Galletto for his help with the sedimentation measurements.

SUPPORTING INFORMATION AVAILABLE

Concentration-dependent intermolecular FRET in samples of ApoE2 (C112S/C158S/A102C) labeled with either Alexa488 or Alexa546 (Figure S1) and concentration dependent quenching of tryptophan fluorescence of WT ApoE4 in the presence of 100 mM acrylamide (Figure S2). This material is available free of charge via the Internet at http://pubs.acs.org.

REFERENCES

1. Corder, E. H., Saunders, A. M., Strittmatter, W. J., Schmechel, D. E., Gaskell, P. C., Small, G. W., Roses, A. D., Haines, J. L., and Pericak-Vance, M. A. (1993) Gene dose of apolipoprotein E type 4 allele and the risk of Alzheimer's disease in late onset families. *Science 261*, 921–923.
2. Drzezga, A., Grimmer, T., Henriksen, G., Muhlau, M., Perneczky, R., Miederer, I., Praus, C., Sorg, C., Wohlschlager, A., Riemenschneider, M., Wester, H. J., Foerstl, H., Schwaiger, M., and Kurz, A. (2009) Effect of APOE genotype on amyloid plaque load and gray matter volume in Alzheimer disease. *Neurology 72*, 1487–1494.
3. Farrer, L. A., Cupples, L. A., Haines, J. L., Hyman, B., Kukull, W. A., Mayeux, R., Myers, R. H., Pericak-Vance, M. A., Risch, N., and van Duijn, C. M. (1997) Effects of age, sex, and ethnicity on the association between apolipoprotein E genotype and Alzheimer disease. A meta-analysis. APOE and Alzheimer Disease Meta Analysis Consortium. *JAMA, J. Am. Med. Assoc. 278*, 1349–1356.
4. Alberts, M. J., Graffagnino, C., McClenny, C., DeLong, D., Strittmatter, W., Saunders, A. M., and Roses, A. D. (1995) ApoE genotype and survival from intracerebral haemorrhage. *Lancet 346*, 575.
5. Wilson, C., Wardell, M. R., Weisgraber, K. H., Mahley, R. W., and Agard, D. A. (1991) Three-dimensional structure of the LDL receptor-binding domain of human apolipoprotein E. *Science 252*, 1817–1822.
6. Hatters, D. M., Peters-Libeu, C. A., and Weisgraber, K. H. (2006) Apolipoprotein E structure: Insights into function. *Trends Biochem. Sci. 31*, 445–454.
7. Westerlund, J. A., and Weisgraber, K. H. (1993) Discrete carboxyl-terminal segments of apolipoprotein E mediate lipoprotein association and protein oligomerization. *J. Biol. Chem. 268*, 15745–15750.
8. Dergunov, A. D., Hoy, A., Smirnova, E. A., Visvikis, S., and Siest, G. (2003) Charge-based heterogeneity of human plasma lipoproteins at hypertriglyceridemia: Capillary isotachophoresis study. *Int. J. Biochem. Cell Biol. 35*, 530–543.
9. Chou, C. Y., Lin, Y. L., Huang, Y. C., Sheu, S. Y., Lin, T. H., Tsay, H. J., Chang, G. G., and Shiao, M. S. (2005) Structural variation in human apolipoprotein E3 and E4: Secondary structure, tertiary structure, and size distribution. *Biophys. J. 88*, 455–466.
10. Perugini, M. A., Schuck, P., and Howlett, G. J. (2000) Self-association of human apolipoprotein E3 and E4 in the presence and absence of phospholipid. *J. Biol. Chem. 275*, 36758–36765.
11. Aggerbeck, L. P., Wetterau, J. R., Weisgraber, K. H., Wu, C. S., and Lindgren, F. T. (1988) Human apolipoprotein E3 in aqueous solution. II. Properties of the amino- and carboxyl-terminal domains. *J. Biol. Chem. 263*, 6249–6258.
12. Patel, A. B., Khumsupan, P., and Narayanaswami, V. (2010) Pyrene fluorescence analysis offers new insights into the conformation of the lipoprotein-binding domain of human apolipoprotein E. *Biochemistry 49*, 1766–1775.
13. Fan, D., Li, Q., Korando, L., Jerome, W. G., and Wang, J. (2004) A monomeric human apolipoprotein E carboxyl-terminal domain. *Biochemistry 43*, 5055–5064.
14. Zhang, Y., Vasudevan, S., Sojitrawala, R., Zhao, W., Cui, C., Xu, C., Fan, D., Newhouse, Y., Balestra, R., Jerome, W. G., Weisgraber, K., Li, Q., and Wang, J. (2007) A monomeric, biologically active, full-length human apolipoprotein E. *Biochemistry 46*, 10722–10732.
15. Yokoyama, S., Kawai, Y., Tajima, S., and Yamamoto, A. (1985) Behavior of human apolipoprotein E in aqueous solutions and at interfaces. *J. Biol. Chem. 260*, 16375–16382.
16. Barbier, A., Clement-Collin, V., Dergunov, A. D., Visvikis, A., Siest, G., and Aggerbeck, L. P. (2006) The structure of human apolipoprotein E2, E3 and E4 in solution 1. Tertiary and quaternary structure. *Biophys. Chem. 119*, 158–169.
17. Munoz, F., Valles, M. A., Donoso, J., Echevarria, G., and Garcia Blanco, F. (1983) Kinetic and thermodynamic study of the tetramerization equilibrium of phosphorylase b. *J. Biochem. 94*, 1649–1659.
18. Kitano, H., Maeda, Y., and Okubo, T. (1989) Kinetic study of the effects of solvation on the dimerization process of α-chymotrypsin. *Biophys. Chem. 33*, 47–54.
19. Lu, H. S., Chang, W. C., Mendiaz, E. A., Mann, M. B., Langley, K. E., and Hsu, Y. R. (1995) Spontaneous dissociation-association of monomers of the human-stem-cell-factor dimer. *Biochem. J. 305* (Part 2), 563–568.
20. Moore, J. M., Patapoff, T. W., and Cromwell, M. E. (1999) Kinetics and thermodynamics of dimer formation and dissociation for a recombinant humanized monoclonal antibody to vascular endothelial growth factor. *Biochemistry 38*, 13960–13967.
21. Veronese, P. K., Stafford, R. P., and Lucius, A. L. (2009) The *Escherichia coli* ClpA molecular chaperone self-assembles into tetramers. *Biochemistry 48*, 9221–9233.
22. Venezia, C. F., Meany, B. J., Braz, V. A., and Barkley, M. D. (2009) Kinetics of association and dissociation of HIV-1 reverse transcriptase subunits. *Biochemistry 48*, 9084–9093.
23. Hoggett, J. G., and Kellett, G. L. (1992) Kinetics of the monomer-dimer reaction of yeast hexokinase PI. *Biochem. J. 287* (Part 2), 567–572.
24. Darke, P. L., Jordan, S. P., Hall, D. L., Zugay, J. A., Shafer, J. A., and Kuo, L. C. (1994) Dissociation and association of the HIV-1 protease dimer subunits: Equilibria and rates. *Biochemistry 33*, 98–105.
25. Chen, M. J., and Mayo, K. H. (1991) Human platelet factor 4 subunit association/dissociation thermodynamics and kinetics. *Biochemistry 30*, 6402–6411.
26. Garai, K., Mustafi, S. M., Baban, B., and Frieden, C. (2010) Structural differences between apolipoprotein E3 and E4 as measured by ^{19}F NMR. *Protein Sci. 19*, 66–74.
27. Magde, D., Elson, E. L., and Webb, W. W. (1974) Fluorescence correlation spectroscopy. II. An experimental realization. *Biopolymers 13*, 29–61.
28. Maiti, S., Haupts, U., and Webb, W. W. (1997) Fluorescence correlation spectroscopy: Diagnostics for sparse molecules. *Proc. Natl. Acad. Sci. U.S.A. 94*, 11753–11757.
29. Garai, K., Muralidhar, M., and Maiti, S. (2006) Fiber-optic fluorescence correlation spectrometer. *Appl. Opt. 45*, 7538–7542.
30. Nitsche, J. M., Chang, H. C., Weber, P. A., and Nicholson, B. J. (2004) A transient diffusion model yields unitary gap junctional permeabilities from images of cell-to-cell fluorescent dye transfer between *Xenopus* oocytes. *Biophys. J. 86*, 2058–2077.
31. Schuck, P., Perugini, M. A., Gonzales, N. R., Howlett, G. J., and Schubert, D. (2002) Size-distribution analysis of proteins by analytical ultracentrifugation: Strategies and application to model systems. *Biophys. J. 82*, 1096–1111.
32. Schuck, P. (2000) Size-distribution analysis of macromolecules by sedimentation velocity ultracentrifugation and Lamm equation modeling. *Biophys. J. 78*, 1606–1619.
33. Selvin, P. R., and Ha, T. (2008) Single-molecule techniques: A laboratory manual, Cold Spring Harbor Laboratory Press, Plainview, NY.

34. Johnson, K. A., Simpson, Z. B., and Blom, T. (2009) Global kinetic explorer: A new computer program for dynamic simulation and fitting of kinetic data. *Anal. Biochem. 387*, 20–29.
35. Johnson, K. A., Simpson, Z. B., and Blom, T. (2009) FitSpace explorer: An algorithm to evaluate multidimensional parameter space in fitting kinetic data. *Anal. Biochem. 387*, 30–41.
36. Hatters, D. M., Zhong, N., Rutenber, E., and Weisgraber, K. H. (2006) Amino-terminal domain stability mediates apolipoprotein E aggregation into neurotoxic fibrils. *J. Mol. Biol. 361*, 932–944.
37. Kellett, G. L., and Gutfreund, H. (1970) Reactions of haemoglobin dimers after ligand dissociation. *Nature 227*, 921–926.
38. Pollard, T. D., and Cooper, J. A. (1986) Actin and actin-binding proteins. A critical evaluation of mechanisms and functions. *Annu. Rev. Biochem. 55*, 987–1035.
39. Noble, R. W., Reichlin, M., and Gibson, Q. H. (1969) The reactions of antibodies with hemeprotein antgens. The measurement of reaction kinetics and stoichiometry by fluorescence quenching. *J. Biol. Chem. 244*, 2403–2411.
40. Ward, E. S., Gussow, D., Griffiths, A. D., Jones, P. T., and Winter, G. (1989) Binding activities of a repertoire of single immunoglobulin variable domains secreted from *Escherichia coli*. *Nature 341*, 544–546.
41. Northrup, S. H., and Erickson, H. P. (1992) Kinetics of protein-protein association explained by Brownian dynamics computer simulation. *Proc. Natl. Acad. Sci. U.S.A. 89*, 3338–3342.
42. Hesse, C., Larsson, H., Fredman, P., Minthon, L., Andreasen, N., Davidsson, P., and Blennow, K. (2000) Measurement of apolipoprotein E (apoE) in cerebrospinal fluid. *Neurochem. Res. 25*, 511–517.
43. Schuck, P. (1998) Sedimentation analysis of noninteracting and self-associating solutes using numerical solutions to the Lamm equation. *Biophys. J. 75*, 1503–1512.
44. Karbassi, F., Quiros, V., Pancholi, V., and Kornblatt, M. J. (2010) Dissociation of the octameric enolase from *S. pyogenes*: One interface stabilizes another. *PLoS One 5*, e8810.
45. Perugini, M. A., Schuck, P., and Howlett, G. J. (2002) Differences in the binding capacity of human apolipoprotein E3 and E4 to size-fractionated lipid emulsions. *Eur. J. Biochem. 269*, 5939–5949.
46. Salter, J. D., Krucinska, J., Raina, J., Smith, H. C., and Wedekind, J. E. (2009) A hydrodynamic analysis of APOBEC3G reveals a monomer-dimer-tetramer self-association that has implications for anti-HIV function. *Biochemistry 48*, 10685–10687.
47. Brown, P. H., Balbo, A., and Schuck, P. (2009) On the analysis of sedimentation velocity in the study of protein complexes. *Eur. Biophys. J. 38*, 1079–1099.
48. Brookes, E., Cao, W., and Demeler, B. (2010) A two-dimensional spectrum analysis for sedimentation velocity experiments of mixtures with heterogeneity in molecular weight and shape. *Eur. Biophys. J. 39*, 405–414.
49. Westley, F., and Cohen, I. (1966) Tables of values relating the axial ratio to the frictional ratio of an ellipsoid of revolution. *Biopolymers 4*, 4.